Frequency-dependent electric dc power consumption model including quantum-conversion efficiencies in ultrafast all-optical semiconductor gates around 160 Gb/s

Jun Sakaguchi[1], Ferran Salleras[1], Kohsuke Nishimura[2] and Yoshiyasu Ueno[1]

[1]University of Electro-Communications, 1-5-1 Chohugaoka, Chohu, Tokyo, Japan
[2]KDDI R&D Laboratories Inc., 2-1-15 Ohara, Kamifukuoka-shi, Saitama 356-8502, Japan
sakaguchi@ultrafast.ee.uec.ac.jp

Abstract: Based on nine up-to-date types of semiconductor-optical-amplifier (SOA) samples, we devised a power-consumption model of SOA-based all-optical gates as a tool to develop faster and more efficient OTDM systems for bitrates from 10 to 160 Gb/s and those over 160 Gb/s. The conventional effect of a continuous wave (cw) holding beam was included in the model. Furthermore, in this work we defined three step-wise quantum conversion efficiencies η_1, η_2, and η_3 from current-injected carriers through photons. The dependence of each of the three efficiencies on the SOA-structure was studied. The total efficiency η_T observed for the nine SOAs ranged widely from 0.07 to 0.46. The validity of the power-consumption model was verified by systematically measuring the effective carrier recovery rate. According to our model, the power consumption of the best existing SOA-based gate for 160-Gb/s signals is 750 mW, and this increases at a rate approximately proportional to (bitrate)^2, and decreases proportionally to $(1/\eta_T)^2$.

OCIS codes: (060.0060) Fiber optics and optical communications; (060.1155) All-optical networks; (120.5060) Phase modulation; (190.5970) Semiconductor nonlinear optics including MQW; (190.7110) Ultrafast nonlinear optics; (250.5980) Semiconductor optical amplifiers; (320.7080) Ultrafast devices; (320.7160) Ultrafast technology.

References and links

1. K. E. Stubkjaer, "Semiconductor optical amplifier-based all-optical gates for high-speed optical processing," IEEE J. Selected Topics in Quantum Electron. **6**, 1428-1435 (2000).
2. Y. Ueno, S. Nakamura, and K. Tajima, "Nonlinear phase shifts induced by semiconductor optical amplifiers with control pulses at repetition frequencies in the 40–160-GHz range for use in ultrahigh-speed all-optical signal processing," J .Opt. Soc. Am. **B19**, 2573-2589 (2002).
3. S. Nakamura, Y. Ueno, K. Tajima, "Error-free all-optical demultiplexing at 336 Gb/s with a hybrid-integrated symmetric-Mach-Zehnder switch," presented at Optical Fiber Communications Conference (2002), FD3.
4. Y. Ueno, S. Nakamura, and K. Tajima, "Penalty-free error-free all-optical data pulse regeneration at 84 Gb/s by using a symmetric-Mach-Zehnder-type semiconductor regenerator," IEEE Photonics. Technol. Lett. **13**, 469-471 (2001).
5. S. Nakamura, Y. Ueno, and K. Tajima, "168-Gb/s all-optical wavelength conversion with a symmetric-Mach-Zehnder-type switch," IEEE Photonics. Technol. Lett. **13**, 1091-1093 (2001).
6. Y. Liu, E. Tangdiongga, Z. Li, S. Zhang, H. de Waardt, G. D. Khoe, and H. J. S. Dorren, "Error-free all-optical wavelength conversion at 160 Gb/s using a semiconductor optical amplifier and an optical bandpass filter," J. Lightwave. Technol. **24**, 230-236 (2006).
7. Y. Liu, E. Tangdiongga, Z. Li, H. de Waardt, A.M.J. Koonen, G.D. Khoe, X. Shu, I. Bennion and H.J.S. Dorren, "Error-free 320-Gb/s all-optical wavelength conversion using a single semiconductor optical amplifier," J. Lightwave. Technol. **25**, 103-108 (2007).

#87129 - $15.00 USD Received 31 Aug 2007; revised 23 Oct 2007; accepted 24 Oct 2007; published 26 Oct 2007

8. E. Tangdiongga, Y. Liu, H. de Waardt, G. D. Khoe, A. M. J. Koonen, H. J. S. Dorren, X. Shu and I. Bennion, "All-optical demultiplexing of 640 to 40 Gbits/s using filtered chirp of a semiconductor optical amplifier," Opt. Lett. **32**, 835-837 (2007).
9. C. Schubert, R. H. Derksen, M. Moller, R. Ludwig, C.-J. Weiske, J. Lutz, S. Ferber, A. Kirstadter, G. Lehmann and C. Schmidt-Langhorst, "Integrated 100-Gb/s ETDM receiver," J. Lightwave Technol. **25**, 122-130 (2007).
10. R. J. Manning and D. A. O. Davies, "Three-wavelength device for all-optical signal processing," Opt. Lett. **19**, 889-891 (1994).
11. J. L. Pleumeekers, M. Kauer, K. Dreyer, C. Burrus, A. G. Dentai, S. Shunk, J. Leuthold and C. H. Joyner, "Acceleration of gain recovery in semiconductor optical amplifiers by optical injection near transparency wavelength," IEEE Photonics Technol. Lett. **14**, 12-14 (2002).
12. G. Talli and M.J. Adams, "Amplified spontaneous emission in semiconductor optical amplifiers: modelling and experiments," Opt. Commun. **218**, 161-166 (2003).
13. G. Talli and M.J. Adams, "Gain recovery acceleration in semiconductor optical amplifiers employing a holding beam," Opt. Commun. **245**, 363-370 (2005).
14. A. E. Siegman, *Lasers* (Oxford Univ. Press, 1986), Chap. 7 and Chap. 10.
15. T. Saitoh and T. Mukai, "Gain saturation characteristics of traveling-wave semiconductor laser amplifiers in short optical pulse amplification," IEEE J. Quantum. Electron. **26**, 2086-2094 (1990).
16. Y. Ueno, M. Toyoda, R. Suzuki and Y. Nagasue, "Modeling of the polarization-discriminating symmetric-Mach-Zehnder-type optical-3R gate scheme and its available degree of random amplitude-noise suppression," Optics Express, **14**, 348-360 (2006).
17. J. Sakaguchi, M.L. Nielsen, T. Ohira, R. Suzuki and Y. Ueno, "Observation of small sub-pulses out of the delayed-interference signal-wavelength converter," Jpn. J. Appl. Phys **44**, L1358-1360 (2005).
18. M. J. Connelly, "Wideband semiconductor optical amplifier steady-state numerical model," IEEE J. Quantum. Electron. **37**, 439-447 (2001).
19. M. L. Nielsen, J. Mork, R. Suzuki, J. Sakaguchi and Y. Ueno, "Experimental and theoretical investigation of the impact of ultra-fast carrier dynamics on highspeed SOA-based all-optical switches," Optics Express **14**, 331-347 (2006).

1. Introduction

All-optical signal-processing gates based on the nonlinearities of semiconductor optical amplifiers (SOAs) are promising devices for future OTDM networks because they are capable of ultrafast signal processing and low power consumption [1,2]. All-optical demultiplexing, 3R regeneration, and wavelength conversion based on cross-phase modulation (XPM) in SOAs have been achieved for operating frequencies exceeding 100 GHz [3-5], and 320- to 640-GHz operation of all-optical SOA gates using ultrafast chirp dynamics has recently been demonstrated [6-8]. These devices typically consumed 0.4 to 1.0 W electrical power, while the latest electrical demultiplexer consumes 5.5 W in 100-GHz operation [9]. As the capabilities of SOAs for ultrafast gating have become clear, the lower limit of electric power consumption and its origin have become important design issues. A practical engineering model that describes dc power consumption has, however, not yet been reported to the best of the authors' knowledge. Because such a model has not been available, it has been very difficult for system researchers to design the total power consumption of the various large-scale 160-Gb/s OTDM systems now under research.

The electrical power consumption of an SOA in an all-optical gate is dominated by two factors: the amount of optical-pulse-induced modulation as the optical phase shift in the case of XPM, and the recovery time of the depleted carrier density after optical modulation. It has long been recognized that the so-called optical holding beam effectively accelerates the carrier's recovery time [10,11], while the holding beam itself consumes a significant part of the injected carriers via the stimulated recombination process and consequently reduces the amount of optical phase shift in the co-propagating optical signal component. It has also been qualitatively well known that to accelerate the recovery time while maintaining the amount of optical phase shift in the 0.3-to-1.0 π range, the carrier injection rate (*i.e.*, the injection current density) must be increased, and this increases in the dc power consumption.

To discuss the power consumption, a detailed understanding of the quantum conversion efficiency from the number of injected carriers to the number of optical-pulse-induced

#87129 - $15.00 USD Received 31 Aug 2007; revised 23 Oct 2007; accepted 24 Oct 2007; published 26 Oct 2007

stimulated recombinations in the SOA is needed. It is reasonably expected that an SOA with low conversion efficiency requires a large current injection for the gating operation. Furthermore, an increase in the injection current density might slightly degrade the quantum conversion efficiency. This quantum efficiency was not taken into account in most previous studies. Some researchers discussed SOA gain within continuous wave (cw) regime and carrier recovery using one conversion efficiency parameter [12,13], but no one has studied how conversion efficiency is influenced by the SOA properties. Furthermore, no study of the conversion efficiency in ultrafast optical gating has been reported, even though this has turned out to be significantly lower than that for cw-light amplification.

In this paper, we explain our development of a practical engineering model that scientifically describes the dc power consumption of an SOA-based all-optical gate as a function of its working frequency up to 160 Gb/s. The validity of this model is verified with one series of measured power consumption values. A model of the holding beam's contribution, which is a part of our power-consumption model, is verified through a series of measured results. In these verification processes, measured parameter values are put into most of the independent model parameters, such as several types of quantum efficiencies. The observed dependence of the measured quantum efficiencies on the SOA structural parameters are also discussed.

2. Our model of carrier conversion efficiency

We define three different carrier conversion efficiencies, and use them to evaluate different carrier losses in the SOA. Figure 1 shows the loss model for injected carriers.

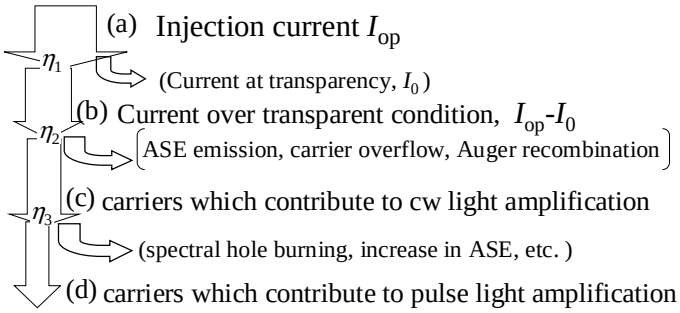

Fig. 1. Loss model of injected carriers. η_1 to η_3 stand for conversion efficiencies.

2.1 Definition of carrier conversion efficiency

We start from the total carrier number N and carrier density n in the active region. When n is below the population inversion threshold n_0, the SOA has a negative gain and shows no band-filling nonlinearity. Thus, the injection current I_{op} should be larger than the transparent current I_0 (where $n=n_0$) and the number of carriers available for the gating should be reduced to the excess carrier number N_{ex}, where $N_{ex}=N-N_0$. For this process, we define the first conversion efficiency η_1 as $\eta_1=N_{ex}/N$.

Next, we introduce the carrier number N_{cw}, which is the maximum number of stored carriers available for amplification of saturating cw light. This can also be understood as the number of carriers available for optical gating at the low frequency limit. N_{cw} is supposed to be smaller than N_{ex} defined above, because of the effects of ASE, Auger recombination, carrier overflow, intervalence band absorption, and free carrier absorption. The second conversion efficiency η_2 is defined as $\eta_2=N_{cw}/N_{ex}$. In this paper, we will not discuss the individual loss contributions, because of the experimental difficulty of determining these.

Finally, we introduce the carrier number N_{pulse}, which is the maximum number of stored carriers available for amplification of ultrafast optical pulses. N_{pulse} is supposed to be smaller

#87129 - $15.00 USD Received 31 Aug 2007; revised 23 Oct 2007; accepted 24 Oct 2007; published 26 Oct 2007

than N_{cw}, and the third efficiency η_3 is defined as $\eta_3=N_{pulse}/N_{cw}$. Its potential causes are spectral hole burning and carrier heating, or increases in ASE recombination caused by the higher average-carrier density compared with the cw-light amplification case, and so on. Note that this difference in SOA reactions to cw light and ultrafast pulses only appears well above the small signal regime, where practical gating operation is carried out. We consider N_{pulse} to have the largest influence on ultrafast gating performance. Therefore, we define the total carrier-conversion efficiency η_T for ultrafast gating as $\eta_T=N_{pulse}/N=\eta_1\eta_2\eta_3$. If the dominant factors of each efficiency can be revealed, we will be able to maximize the total efficiency by improving each contribution separately.

2.2 Characterization of the conversion efficiency

We suppose that the carrier numbers and conversion efficiencies defined above can be characterized from fundamental SOA parameters as follows. When the carrier loss rate is $1/\tau_C$ and the total carrier number is N, the carrier loss N/τ_C should balance the injection flow I_{op}/q (q: elemental charge). Thus, the total carrier number N can be estimated as

$$N=\frac{I_{OP}}{q}\tau_C. \tag{2.1}$$

η_1 and the excess carrier number are supposed to be given by the transparency current I_0 as

$$\eta_1=\frac{N_{ex}}{N}=\frac{I_{OP}-I_0}{I_{OP}}. \tag{2.2}$$

Here, we should mention that N and N_{ex} obtained from these relations contain certain underestimations when the dependence of the carrier loss rate on the injection current is large. We will discuss it in Section 3.

N_{cw} is supposed to be obtained from the gain-saturation measurement of the SOA for cw light. As the intensity of the input light increases, the SOA chip gain G decreases from the small signal gain (SSG) G_0. For an SOA with saturation power P_{sat}^{cw}, G is suppressed by 3 dB when the output power reaches $P_{3dB}=P_{sat}^{cw}\cdot\ln 2$. Taking the conventional discussion [14,15] regarding the gain saturation into account, we relate N_{cw} to P_{sat}^{cw}, G_0 and the carrier lifetime τ_C as

$$\eta_2=\frac{N_{cw}}{N_{ex}},\qquad N_{cw}=\frac{P_{sat}^{cw}\tau_C}{h\nu}\ln G_0^{cw}. \tag{2.3}$$

Similarly, N_{pulse} is supposed to be obtained from the gain-saturation measurement of the SOA for ultrafast pulses. If the injected pulse train has a much longer interval than τ_C, the net gain of the pulse will be as follows:

$$G^{pulse}(E_{out})=\frac{E_{out}}{E_{sat}^{pulse}}\frac{1}{\ln\left\{\exp\left(E_{out}/E_{sat}^{pulse}\right)+G_0-1\right\}-\ln G_0}. \tag{2.4}$$

The pulse saturation energy E_{sat}^{pulse} can be obtained from the 2.35-dB suppression point, and we relate it to N_{pulse} as follows:

$$\eta_3=\frac{N_{pulse}}{N_{cw}},\qquad N_{pulse}=\frac{E_{sat}^{pulse}}{h\nu}\ln G_0^{pulse}. \tag{2.5}$$

#87129 - $15.00 USD Received 31 Aug 2007; revised 23 Oct 2007; accepted 24 Oct 2007; published 26 Oct 2007

Table 1. List of SOA samples and their structure

Sample	Type	Active region length, L_{eff} (μm)	Active region width, w_A (μm)	Active region thickness, d_A (μm)	Confinement factor, Γ
A#1	Bulk	1000	2	0.1	0.1~0.2
A#2		700			
A#3		300			
A#4		700			
B#1	MQW	1100 (*1)	1.25	0.038 (*2)	~0.2
B#2		700 (*1)			
B#3		500 (*1)			
C#1	Bulk	700	1.2	0.2	0.3~0.4
D#1	Bulk	1500	0.6	0.35	0.5

(*1) Effective length, considering 50 % contribution from taper regions

(*2) Sum of well thickness

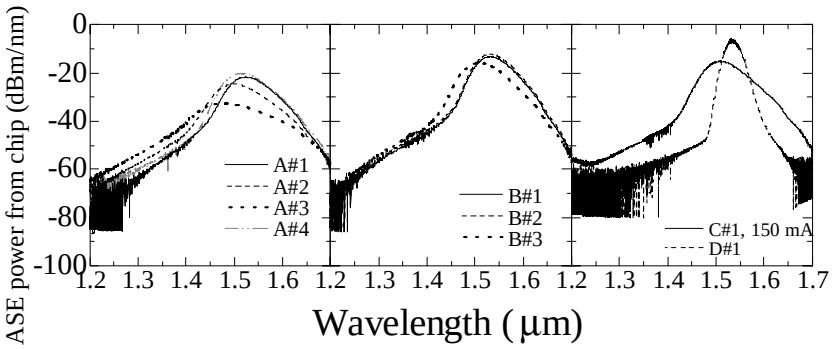

Fig. 2. Measured ASE spectra of SOA samples at I_{OP} = 200 mA.

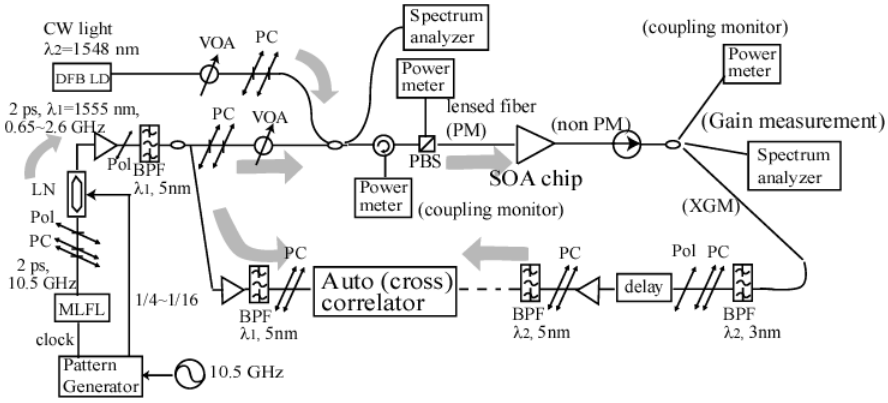

Fig. 3. Experimental setup for SOA chip characterization. VOA: variable optical attenuator, Pol: polarizer, PC: polarization controller, PBS: polarizing beam splitter, BPF: band-pass filter, MLFL: mode-locked fiber laser

#87129 - $15.00 USD Received 31 Aug 2007; revised 23 Oct 2007; accepted 24 Oct 2007; published 26 Oct 2007

The intrinsic difference between N_{cw} and N_{pulse} seems to be overlooked in the conventional gain-saturation theory. In the new rate equation model (see Section 4), both cw and pulse saturation are modeled as independent characteristics.

3. Conversion efficiency measurement and results

To evaluate the carrier conversion efficiency of actual SOAs, we measured the fundamental parameters of several custom-designed SOA chips and commercial modules from different manufacturers (A to D). Attributes of the SOA samples and examples of ASE spectra are shown in Table 1 and Fig. 2, respectively. For series A and B, we prepared chips with different (effective) active-region lengths L_{eff}. For each custom-designed chip, except for the shortest one (A#3), more than two wires per electrode were bonded to enable injection currents over 500 mA.

The typical setup for SOA-chip characterization is shown in Fig. 3. We coupled lensed fibers to the input and output facets of the chip using precision stages, and obtained 2- to 5-dB coupling losses for each facet. Temperature was stabilized at close to 25°C. The ASE intensities from both facets were continuously monitored by power meters, and through careful adjustment of the couplings fluctuations were kept below 0.2 dB. First, we measured the cw-gain by using a DFB-LD (λ_2= 1548 nm) and an optical spectrum analyzer. Figure 4 plots the measured SSG of each sample against I_{OP}. The transparent currents I_0 were obtained from these results. Figure 5(a) shows typical gain-saturation profiles. We obtained P_{sat}^{cw} as a function of I_{OP} from the 3-dB suppression points. As can be seen in Fig. 6(a), P_{sat}^{cw} increased

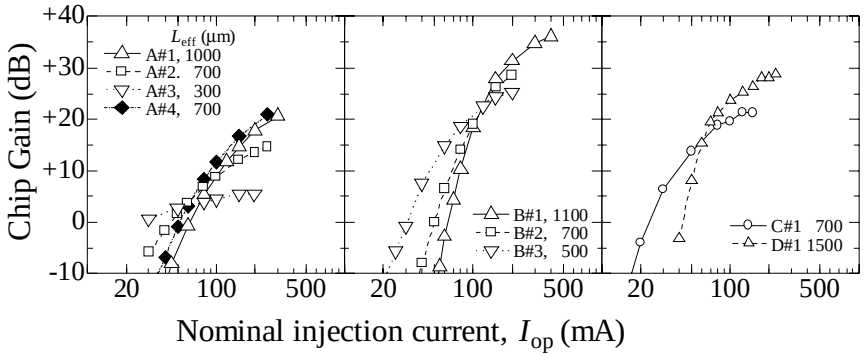

Fig. 4. Measured small-signal gains of SOA samples versus current. Sample details are given in Table 1. Gains were measured with cw light, λ_2=1548 nm. Input cw power into each chip was kept under –30 dBm.

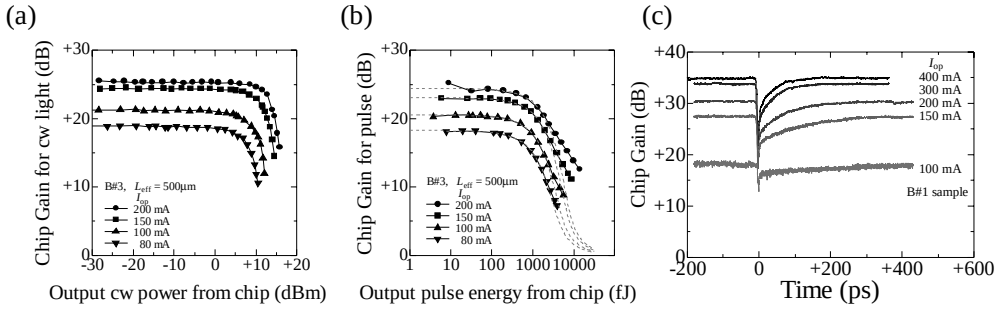

Fig. 5. Typical SOA chip characteristics (a) Gain-saturation profiles for cw light. (b) Gain-saturation profiles for ultrafast pulses (2-ps width, 0.65-GHz repetition). The dashed lines in (b) show the theoretical fit using Eq. (2.4). (c) Typical XGM profiles measured with a cross correlator. The cw-probe intensity and pulse energy into the chip were set to –25 dBm and 10 fJ, respectively.

#87129 - $15.00 USD Received 31 Aug 2007; revised 23 Oct 2007; accepted 24 Oct 2007; published 26 Oct 2007

almost linearly with I_{OP} without convergence. The SOA gains for ultrafast pulses were measured for each sample. To obtain ultrafast optical pulses with lower frequency than $1/\tau_C$, we used a mode-locked fiber laser (MLFL: Pritel Inc., UOC-3) with an external $LiNbO_3$ modulator. Pulses with a 2-ps width, λ_1=1555 nm, and 10.5-GHz frequency from the MLFL were modulated down to a 0.65-GHz pulse train. We monitored the auto-correlation trace of the pulse train so that we could keep its extinction ratio above 20 dB. Typical gain-saturation profiles are shown in Fig. 5(b). We see that for each I_{OP}, the SSGs for the cw input are almost the same as for ultrafast pulses. We fitted the measured profiles to Eq. (2.4), and they showed good agreement up to E_{out} ~ 3000 fJ. The difference at E_{out} > 3000 fJ was probably caused by the slight residual of the 10.5-GHz pulses. From the fit results, we obtained E_{sat}^{pulse} of each SOA as a function of I_{OP} (Fig. 6(b)). In contrast to the case of P_{sat}^{cw}, they converged as I_{OP} increased.

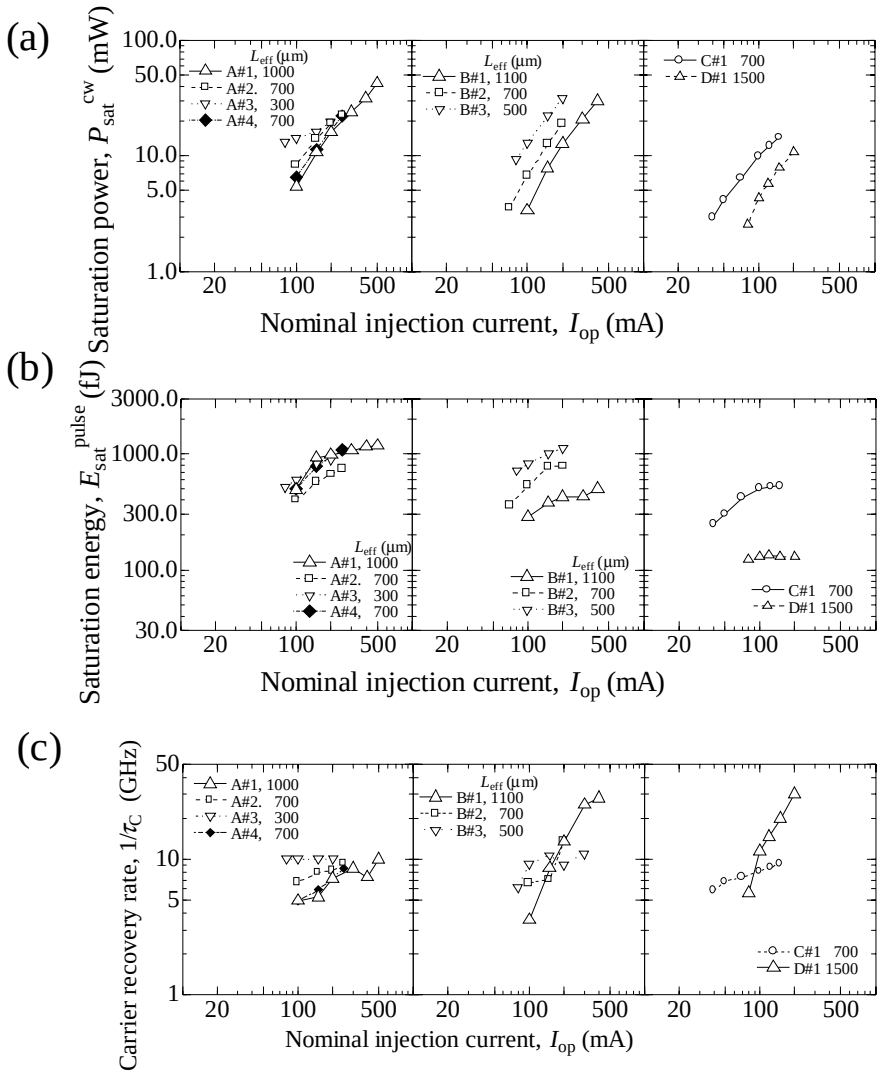

Fig. 6. Measured SOA parameters used for evaluation of the conversion efficiencies (a) Saturation power of SOA chips versus current for cw light. (b) Saturation energy for ultrafast pulses (2-ps width, 0.65 GHz). (c) Carrier-recovery rate $1/\tau_C$.

#87129 - $15.00 USD Received 31 Aug 2007; revised 23 Oct 2007; accepted 24 Oct 2007; published 26 Oct 2007

The carrier recovery rates $1/\tau_C$ of each SOA at several injection currents were determined from XGM measurements using a cross-correlator (Femtochrome Research Inc., FR-103XR) and mode-locked pulses modulated down to 1.3 GHz. External variable delays and an elaborate calibration process were used to expand the scan range to 600 ps. The intensity of the probe cw light was typically set to -25 dBm to suppress the holding beam effect. Pulse energies into each SOA chip were adjusted within 10~500 fJ so that no gain modulation due to residual 10.5-GHz pulses appeared. Figure 5(c) shows examples of measured XGM waveforms. We can see two recovery processes after gain depletion. From the slower process, we obtained $1/\tau_C$ (Fig. 6(c)). In one exception, we assumed τ_C~100 ps for sample A#3 without fitting, since its small gain seriously degraded the S/N ratio of the output signal and prevented a precise determination of τ_C. From Fig. 6(c), we see that the SOA samples can be categorized into two types: the recovery rates of B#1 and D#1 increased rapidly to 30 GHz with I_{OP}, while those of the others increased slowly around 5 to10 GHz.

Using the measured fundamental parameters, we calculated the conversion efficiencies (Fig. 7). The efficiency values for each sample at I_{OP} = 200 mA were η_1 = 0.68 to 0.87, η_2 = 0.17 to 1.30, η_3 = 0.29 to 0.53, and η_T = 0.07 to 0.40. These values indicate that total efficiency η_T strongly depends on the SOA structure. This dependence resulted mostly from η_2. The B-series MQW samples had a much larger η_2 than the other bulk samples. Among the A-series, the longer chips had a larger η_2, whereas the B-series showed the opposite η_2 dependence on L_{eff}. The reason for this difference is unclear. η_1 depends on I_0, and decreases with L_{eff} since I_0 is proportional to L_{eff}. η_3 was significantly smaller than unity. The results in Fig. 7(c) indicate that η_3 decreases as I_{OP} goes above the optimum condition, and that longer SOAs tend to have larger η_3 values at large I_{OP}. The total efficiency η_T of longer SOAs also tends to be higher at large I_{OP}. Sample B#1 will be the most economical device for I_{OP} ~ 400 mA (η_T ~0.34), while B#3 has the best efficiency for I_{OP} ~ 150 mA (η_T ~0.46).

There appears to be a problem with the definition of N_{ex} using Eqs. (2.1) and (2.2), since the calculated η_2 sometimes exceeds unity. This underestimation of N_{ex} will be reduced if we use another definition as

$$N_{ex} = \int_{I_0}^{I_{OP}} \frac{\tau_C(I)}{q} dI, \tag{3.1}$$

taking into acount that the carrier lifetime τ_C, which is related to the differential carrier injection rate, decreases with the injection current. Determination of N_{ex} using Eq. (3.1) is difficult, however, because it requires precise measurement of τ_C at small I_{OP}. Then we think using Eqs. (2.1) and (2.2) is not a concern and appropriate since the idea is to get a rough understanding of the SOA-characteristics.

Thus, our interpretation of the dependence of the efficiencies on the SOA structure can be summarized as follows. First, the MQW structure is advantageous for increasing η_2. A longer active region decreases η_1, increases or decreases η_2, and increases both η_3 and total efficiency at large I_{OP}. We could not obtain conclusive results for width, thickness or confinement factor, though some of these factors seemed to significantly affect efficiencies. Although these results are useful, we will need to perform more systematic characterizations before we can completely understand the SOA-structure effects.

4. Estimation of SOA electrical power consumption of all-optical gating

Here we propose a model for determining the electrical power requirements of SOAs used in ultrafast all-optical gates. First, we discuss the carrier dynamics of SOAs. Then, we estimate the power consumption from the calculated carrier dynamics. Finally, we compare the calculated power consumption with measured results.

4.1 Rate equation model including conversion efficiencies

#87129 - $15.00 USD Received 31 Aug 2007; revised 23 Oct 2007; accepted 24 Oct 2007; published 26 Oct 2007

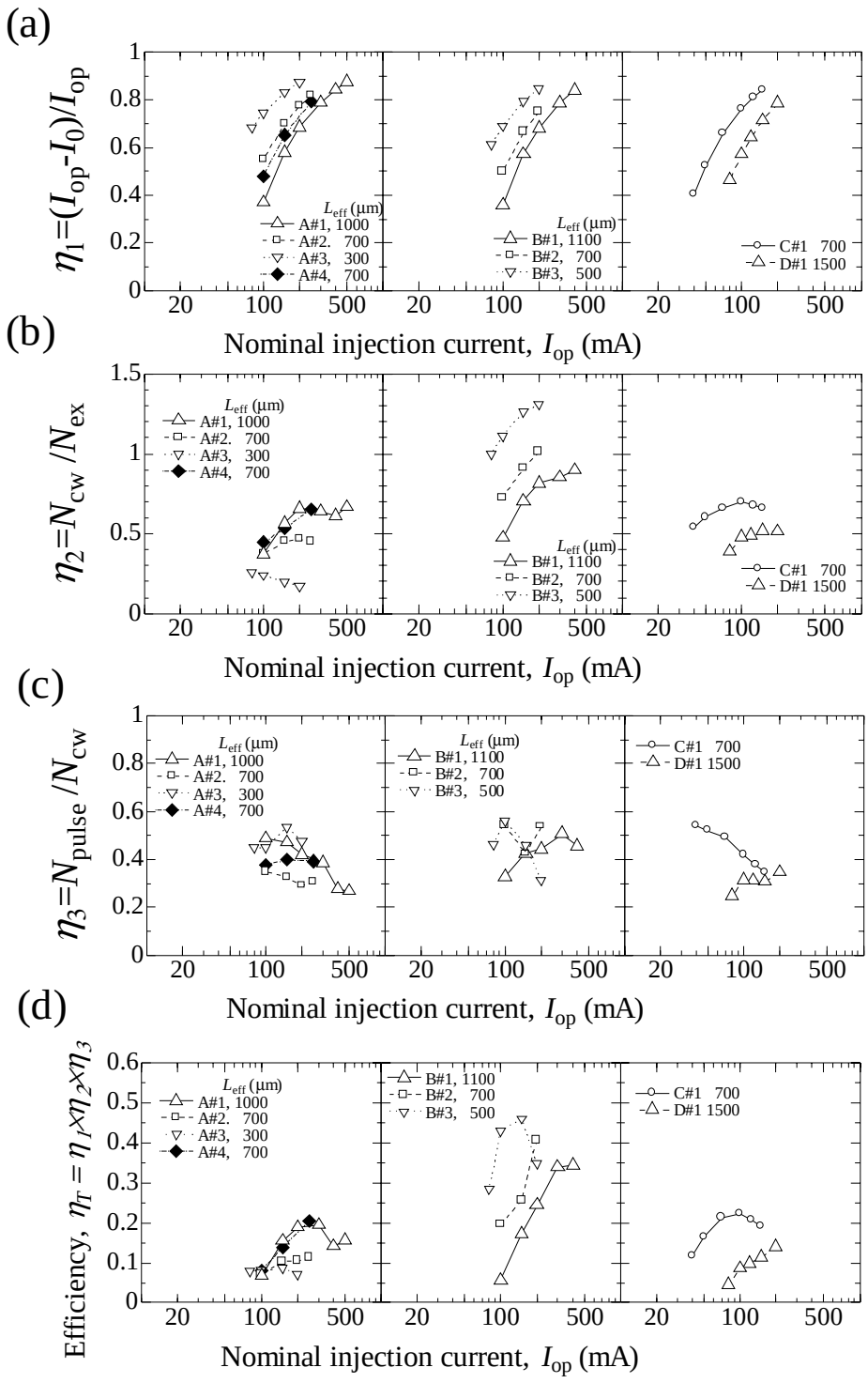

Fig. 7. Measured dependence of SOA sample conversion efficiency on I_{OP}

(a): η_1, (b): η_2, (c): η_3, according to Eqs. (2.2) to (2.5), and (d): total efficiency $\eta_T=\eta_1\times\eta_2\times\eta_3$.

#87129 - $15.00 USD Received 31 Aug 2007; revised 23 Oct 2007; accepted 24 Oct 2007; published 26 Oct 2007

In our preceding analyses, we used a single rate equation to calculate the carrier-density modulation in one SOA module [2,16]. This is a simple but powerful tool to explain the gating characteristics in the time domain [17]. To account for the effect of the three different conversion efficiencies, we expanded the rate equation to the following form:

$$\frac{dn_{pulse}}{dt} = \frac{I_{op}}{qV}\eta_1\eta_2\eta_3 - \frac{n_{pulse}}{\tau_C} - \eta_3\left\{\exp\left(\Gamma L_{eff}\frac{dg^{cw}}{dn}n_{pulse}\right)-1\right\}\frac{P_{cw}}{\hbar\omega V} - \left\{\exp\left(\Gamma L_{eff}\frac{dg^{pulse}}{dn}n_{pulse}\right)-1\right\}\frac{P_{pulse}}{\hbar\omega V} \quad (4.1)$$

($n_{pulse}=N_{pulse}/V$: carrier density available for ultrafast gating, P_{pulse} and P_{CW}: input light intensities, L_{eff} and $V=L_{eff}\,w_A\,d_A$: active region effective length and volume, Γ: confinement factor, dg/dn: differential gain). Note that η_3 is multiplied by the cw-light term, in view of the difference between n_{pulse} and n_{cw} (the carrier density available for cw light). Both cw gain and pulse gain were supposed to be determined by n_{pulse}, since we did not observe much difference between them unless gain saturation occurred (Fig. 5). We also supposed there are reserved carriers ($n_{reserve}=n_{cw}-n_{pulse}$) which do not explicitly affect gain, and ($1-\eta_3$) of the photons are converted from reserved carriers through intraband interactions in the case of cw-light amplification. This rate-equation model can explain the experimental results regarding the gain saturation for ultrafast pulses quite well, and those regarding the cw-gain saturation up to 3-dB suppression points (Fig. 8(a)). For stronger cw light, other theories may provide better predictions of the gain suppression [18].

The rate equation can be used to calculate the optical carrier modulation and nonlinear phase shift. Injection of P_{pulse} causes carrier recombination Δn_{pulse}, and the nonlinear phase shift is given by

$$\Delta\Phi = k_0\, dn_r/dn\,\Gamma L_{eff}\Delta n_{pulse} \quad (4.2)$$

(k_0: wave number in vacuum, n_r: refractive index).

To verify the model, we simulated the SOA characteristics under holding-beam injection. We used the measured values of η and τ_C at each I_{OP}, and extracted dg^{cw}/dn and dg^{pulse}/dn from the corresponding SSG values. Figure 8(b) shows measured and calculated results for the effective carrier recovery rate of sample B#3 accelerated by the holding-beam. Figure 8(c) shows measured and calculated results for pulse-gain saturation with and without a holding beam. We see that both results approximately agree with each other.

Table 2. Estimated refractive index change of each sample, and related parameters.

Sample	Refractive index change, dn_r/dn_{pulse} (10^{-20} cm^3)	Carrier density for gating, n_{pulse} (10^{18} cm^{-3}) (*2)	Differential gain, dg^{cw}/dn_{pulse} (10^{-17} cm^2) (*2)	Confinement factor, Γ (*3)
A#1	3.8	0.17	142	0.2
A#2	3.8 (*1)	0.11	196	
A#3	3.8 (*1)	0.15	136	
B#1	1.4	0.43	76	0.2
B#2	1.2	1.0	42	
B#3	0.7	2.0	30	

(*1) Estimated from the value for sample A#1.

(*2) Typical values measured at I_{OP} = 200 mA are shown.

(*3) Assumed in view of the values in Table 1.

#87129 - $15.00 USD Received 31 Aug 2007; revised 23 Oct 2007; accepted 24 Oct 2007; published 26 Oct 2007

We also compared measured and calculated nonlinear phase shifts for samples A#1 and B#1 to #3. These can be experimentally determined from XPM spectra out of the SOA [2,19]. The chosen pulse frequency was either 2.6 GHz or 10.5 GHz, depending on the carrier recovery rate of the SOA. dn_r/dn was estimated for each sample from the measured phase shifts at I_{OP} = 200 mA (Table 2). The difference between samples seemed to be negatively correlated to the typical carrier densities. The SOA simulation could approximately reproduce the measured nonlinear phase shifts at various I_{OP}, P_{CW} and P_{pulse} values (Fig. 8(d)), and our model seems feasible for power-consumption simulations.

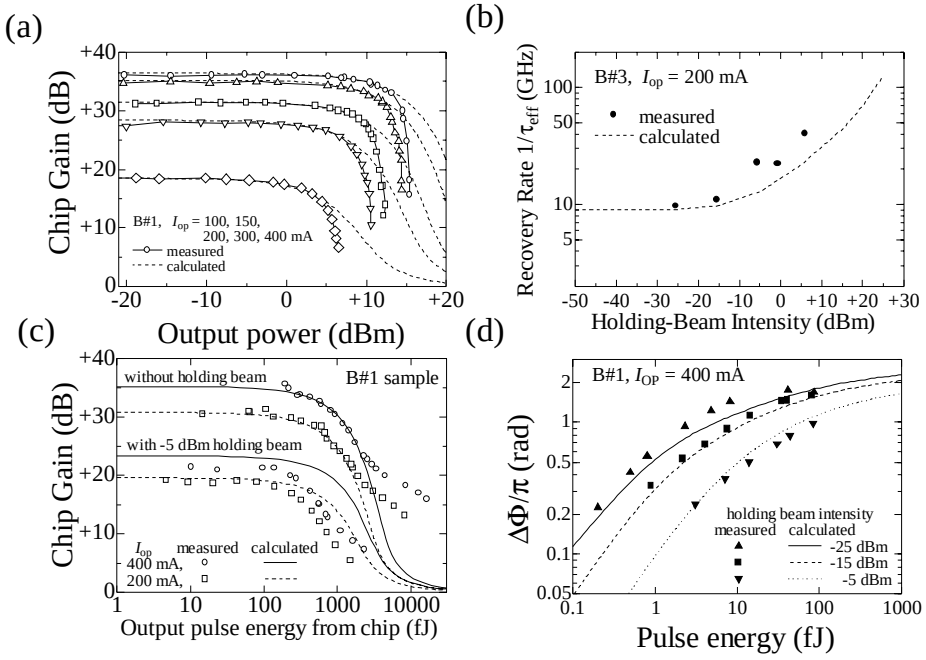

Fig. 8. Comparison of measured and calculated SOA properties under holding-beam injection.

(a) Cw-gain saturation, (b) effective carrier recovery rate $1/\tau_{eff}$, (c) gain saturation for a 2-ps pulse, and (d) nonlinear phase shift $\Delta\Phi$ caused by ultrafast pulses.

4.2 Electrical power consumption

We calculated the correspondence between the electrical power consumption P_{OP} and the operating frequency B for an SOA used in an XPM-based all-optical gate as follows. First, we fixed the control pulse energy $E_{pulse} \equiv \int_{-\infty}^{\infty} P_{pulse} dt$ at a realistic value (340 fJ). Then, for each I_{OP} condition we calculated the induced $\Delta\Phi$ as a function of the holding beam intensity. The required amount of $\Delta\Phi$ depends on the function of the gate: for 3R regeneration or wavelength conversion it is ~0.3π [16]. Therefore, for each I_{OP}, the equation $\Delta\Phi$ = 0.3π provides the maximum available holding-beam intensity P_{CW}. The carrier recovery rate $1/\tau_{eff}$ for this condition can be interpreted as the approximate frequency limit B of the gate. P_{OP} was calculated from I_{OP} using empirical *V-I* characteristics.

Before discussing the power consumption of actual SOAs, we will look at calculated values using non-empirical parameter sets to find their dominant factors. Figure 9 shows our results. Here, the dependences of dg/dn, η and τ_C on I_{OP} were ignored, in contrast to the cases shown in Figs. 8 or 10. Calculations were done down to nearly the low power limits, where $\Delta\Phi$ = 0.3π can be satisfied only when P_{CW} = 0. We found that the maximum frequency is

#87129 - $15.00 USD Received 31 Aug 2007; revised 23 Oct 2007; accepted 24 Oct 2007; published 26 Oct 2007

almost proportional to the total conversion efficiency η_T and dg/dn, but not sensitive to the intrinsic carrier recovery rate $1/\tau_C$. As for the conversion efficiencies of each process, η_3 affects the required holding-beam intensity as well as B. As long as we keep the SOA parameters constant, I_{OP} increases almost linearly with B, so P_{OP} increases with B^2.

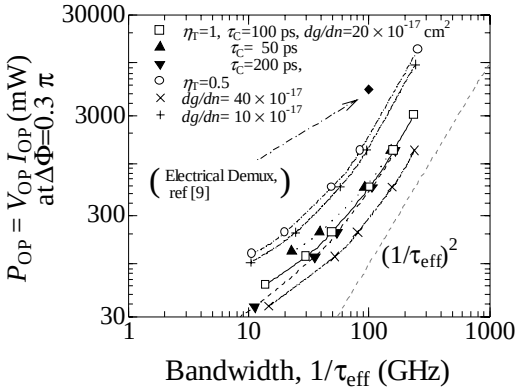

Fig. 9. Calculated power consumption of SOAs versus their maximum operating frequencies when SOA parameters are independent of I_{OP} (Table 3)

Table 3. Parameters assumed for Fig. 9

Symbol	Description	Value
L_{eff}	active region length	1000 μm
w_A	width	1 μm
d_A	thickness	0.05 μm
Γ	confinement factor	0.2
dg^{cw}/dn	differential gain for cw	20.0×10^{-17} cm^2
dg^{pulse}/dn	differential gain for pulse	20.0×10^{-17} cm^2
τ_C	carrier recovery rate without acceleration	100 ps
dn_r/dn_{pulse}	refractive index change	0.4×10^{-20} cm^3
η_T	total carrier-conversion efficiency	1.0

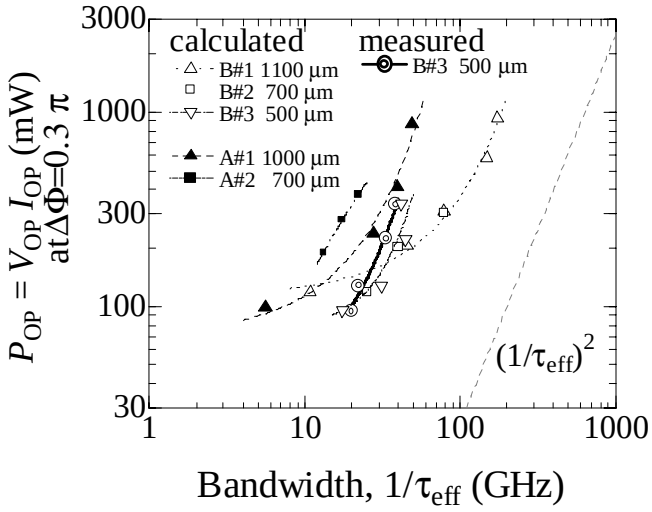

Fig. 10. SOA electrical-power consumption versus carrier recovery rate under holding-beam acceleration. Calculated results using the measured parameters for each sample and measured results for sample B#3 are shown. A control pulse with a 2-ps width and 340-fJ energy was used.

Figure 10 shows the calculated power consumption for the SOA samples. We used the SOA parameters from Section 4.1. The B-series shows better performance than the A-series. When P_{OP} is small, B#3 has the best performance around 20 GHz. As the target frequency increases to over 100 GHz, B#1 becomes preferable. The power consumption of B#1 at 160 GHz is about 750 mW. This is comparable to the power consumption, about 400 mW, of the latest XPM-based 160-Gb/s wavelength conversion [5] or wavelength conversion using ultrafast chirp dynamics [6]. For the A-series, the longer sample had a higher frequency, and the shortest sample A#3 could not achieve $\Delta\Phi = 0.3\pi$ under the injection-current limit. These characteristics result from those of η_T as discussed in Section 3. Except for the difference in

#87129 - $15.00 USD Received 31 Aug 2007; revised 23 Oct 2007; accepted 24 Oct 2007; published 26 Oct 2007

scale, most of the P_{OP}-B profiles in Fig. 10 resemble the corresponding P_{OP}-$1/\tau_C$ profiles. This is due to the complicated correlations of SOA parameter changes. Consequently, P_{OP} of A#1 and B#1 increase with B^2 within the range of about 300 to 1000 mW, and the corresponding values of the others likely increase faster than that. Further discussion requires measurement of the efficiencies at larger P_{OP}.

To prove the validity of our power-consumption model, we measured P_{OP} and $1/\tau_{eff}$ at $\Delta\Phi = 0.3\pi$ for sample B#3 (Fig. 10). We obtained good agreement between the measured and calculated results. Hence, we believe that our model produces satisfactory results as an initial power-consumption model, although it can be improved.

4.3 High-frequency limit

To discuss the future of photonic networks, it is useful to express the B-P_{OP} relation with a simple formula. In this section, we therefore derive an analytical expression for the high-frequency limit.

First, we assume that both the injection current I_{OP} and holding-beam power P_{CW} are large. P_{CW} is chosen according to I_{OP} so that $\Delta\Phi$ stays at a fixed value, as in Section 4.2. Without control pulses the carrier density reaches an equilibrium at $n_{pulse} = n_{eq}$. The small difference in dg^{cw}/dn and dg^{pulse}/dn is ignored for simplicity, and the saturated SOA gain is expressed as

$$G_{eq} = \exp\left(\Gamma L_{eff} \frac{dg}{dn} n_{eq}\right). \tag{4.3}$$

Note that we can approximately suppose that G_{eq} does not change with I_{OP}, because of the constraint on $\Delta\Phi$. The reason is as follows: The number of carrier-to-photon conversions when a control pulse is injected into the SOA in the steady state is given from the net gain of the pulse G_{pe} and E_{pulse}:

$$\Delta n_{pulse} \approx \frac{G_{pe} - 1}{\hbar\omega V} E_{pulse} \tag{4.4}$$

as long as the pulse width is short enough compared to the carrier relaxation time. Then, G_{pe} can be roughly estimated from G_{eq}. Since $\Delta\Phi$ is given from Δn_{pulse} by Eq. (4.2), we can transform Eq. (4.4) into

$$G_{eq} \approx G_{pe} \approx 1 + \frac{\hbar\omega V \Delta\Phi}{E_{pulse}\Gamma L_{eff} k_0 \frac{dn_r}{dn}}. \tag{4.5}$$

Both $\Delta\Phi$ and E_{pulse} are regarded as constant when we obtain the B-P_{op} relation. We also assume that dn_r/dn does not depend on I_{OP}. Therefore, we can approximately regard G_{eq} as constant. For example, $\Delta\Phi = 0.3\pi$ and E_{pulse}=340 fJ result in G_{pe}= 2.5 for sample B#1.

By assuming a steady state and taking only terms including I_{OP} or P_{CW} in Eq. (4.1), we obtain the following relation from Eqs. (4.1) and (4.3):

$$\frac{P_{CW}}{\hbar\omega V} \approx \frac{\eta_T I_{OP}}{\eta_3 (G_{eq} - 1) qV} \tag{4.6}$$

The operating frequency limit can then be obtained as follows: After first-order expansion of Eq. (4.1) in terms of n_{pulse} around n_{eq}, the relaxation of the carrier density deviation $\Delta n(t) = n_{pulse}(t) - n_{eq}$ after the control-pulse injection can be expressed as

$$\begin{aligned} \frac{d(\Delta n(t))}{dt} &= -\frac{\Delta n}{\tau_C} - \eta_3 \frac{G_{eq}\Gamma L_{eff}}{\hbar\omega V} \frac{dg}{dn} P_{CW} \Delta n \\ &= -B \cdot \Delta n. \end{aligned} \tag{4.7}$$

#87129 - $15.00 USD Received 31 Aug 2007; revised 23 Oct 2007; accepted 24 Oct 2007; published 26 Oct 2007

After substituting Eq. (4.6) into the above, we obtain

$$B \approx \frac{1}{\tau_C(I_{OP})} + \frac{G_{eq}}{G_{eq}-1}\frac{\Gamma L_{eff}}{qV}\frac{dg}{dn}(I_{OP})\cdot\eta_T(I_{OP})\cdot I_{OP}. \tag{4.8}$$

When $1/\tau_C$ converges to a finite value as I_{OP} increases, the second term will dominate. The applied voltage V_{op} approaches RI_{OP} (R: resistance). Then, when we assume both dg/dn and η_T are independent of I_{OP}, P_{OP} is expressed as

$$P_{OP} \approx R\left(\frac{G_{eq}-1}{G_{eq}}\frac{qV}{\Gamma L_{eff}}\right)^2\left(\frac{dg}{dn}\right)^{-2}\eta_T{}^{-2}B^2$$

$$= \text{constant}\times B^2. \tag{4.9}$$

Therefore, the B-P_{op} relation will be quadratic under the above assumption. This explains the Fig. 9 results. The total conversion efficiency has an inverse-square contribution to P_{OP} for the actual SOA, so it should be elaborately optimized to reduce the dc power consumption.

5. Conclusion

We developed a new model of the electrical power consumption of SOAs used in ultrafast all-optical gates. The dominant factors of this model are three different carrier-conversion efficiencies and the differential gain of the SOA.

To predict power consumption we measured the conversion efficiencies of current SOAs with our original method. They were η_T = 0.07 to 0.46 in total. A systematic study of the efficiencies of SOAs with different structures revealed that a longer SOA with an MQW structure will have high conversion efficiency at a high injection current. Further study is needed with this method to understand the dependences on the SOA width, thickness, and confinement factor, and through such studies we hope to design a more efficient SOA in the near future.

We calculated the power consumption P_{OP} as a function of operating frequency limit B, based on our power consumption model and measured SOA parameters. We obtained good agreement between the calculated and measured results. A longer SOA with an MQW structure should consume less electric power when the operation frequency is about 100 GHz. The calculated power consumption at 160 Gb/s for our best SOA (B#1) was 750 mW, and it is comparable to experimental values in the literature. At high bit-rate, P_{OP} will increase as B^2 or even faster, depending on the decrease in the conversion efficiencies and differential gain. We believe that the dc power-consumption model that we have developed in this work can be extrapolated to higher frequencies, for example to the 400 to 640 Gb/s range. Such design extrapolation will help material, device, and system researchers in these fields to develop their visions regarding ultrafast, all-optical signal-processing systems in the near future at and beyond the 160-Gb/s level.

Acknowledgements

We thank Mr. Tomonori Yazaki in KDDI Research Laboratories for his valuable technical discussions and supports regarding some of the SOA samples. This work was supported by research project grant #B15360027, “Optical logic gates in the sub-terahertz frequency region,” of the Ministry of Education (MEXT) and the research project grant, “Ultra-low-power and ultrafast optical memory/switching device,” of the New Energy and Industrial Technology Development Organization (NEDO).

#87129 - $15.00 USD Received 31 Aug 2007; revised 23 Oct 2007; accepted 24 Oct 2007; published 26 Oct 2007